Nano Energy 41 (2017) 765–771

Contents lists available at ScienceDirect

Nano Energy

journal homepage: www.elsevier.com/locate/nanoen

Full paper

Hydrogen oxidation reaction in alkaline media: Relationship between electrocatalysis and electrochemical double-layer structure

Nagappan Ramaswamy[1], Shraboni Ghoshal, Michael K. Bates[2], Qingying Jia, Jingkun Li, Sanjeev Mukerjee*

Northeastern University Center for Renewable Energy Technology, Department of Chemistry and Chemical Biology, 317 Egan Research Center, 360 Huntington Avenue, Northeastern University, Boston, MA 02115, USA

ARTICLE INFO

Keywords:
Hydrogen oxidation reaction
Alkaline electrocatalysis
Alkaline membrane fuel cells
Electrochemical double-layer structure
Quasi-specific adsorption
X-ray absorption spectroscopy

ABSTRACT

Enhancing the sluggish kinetics of electrochemical hydrogen-oxidation reaction in high pH environments is of crucial importance considering its applications in alkaline-membrane fuel cells (AMFC) and regenerative hydrogen electrodes for energy storage. Alkaline H_2-oxidation to form water involves reaction between H-adsorbed intermediates and hydroxide anions wherein the nature/source of the latter plays a crucial role. Here, we take a systematic approach to understand why H_2-oxidation kinetics is slower in alkaline media compared to acid. While recently reported models focus on surface-adsorbate bond strength optimization, we herein show that the alkaline H_2-oxidation mechanism is fundamentally different due to a complex interplay between electrocatalysis and electrochemical double-layer structure. A heretofore unknown modern rendition of the double-layer structure is proposed wherein specifically adsorbed (M-OH_{ad}) and quasi-specifically adsorbed (M-$H_{ad/upd}$···$OH_{q\text{-}ad}$) reactive hydroxide-species localized in the compact part of the electrochemical double-layer is shown to define H_2-oxidation kinetics on monometallic and bimetallic catalyst surfaces at high pH.

1. Introduction

Electrocatalysis of hydrogen oxidation reaction (HOR) in zero-emission electrochemical energy conversion devices, in conjunction with renewable sources of H_2 generation, constitutes a vital technological strategy towards fixing the twin challenge of energy security and climate change [1,2]. Proton-exchange and hydroxide-exchange membrane fuel cell devices that operate in low and high pH environments, respectively, provide such clean energy conversion options. A significant challenge to the commercialization of acidic fuel cells is the need for precious-group metal (PGM) electrocatalysts in the low pH environment. U.S Department of Energy cost target demands the total fuel cell system to be < \$30/kW (for an 80 kW_{net} system at 0.125 kW/g_{pgm} equaling 10 g_{pgm}/vehicle), out of which the electrocatalyst represents the single largest expensive component in the stack [3,4]. Recent advancements in alkaline membrane electrolytes that enable hydroxide-anion transport at useful conductivity values of 20–40 mS cm^{-1} provide an avenue for the application of non-precious catalyst materials for cost-effective fuel cell development [5–9].

Despite these new opportunities, several key questions in alkaline electrocatalysis remain unanswered. For instance, HOR at high pH is a kinetically sluggish process characterized by two to three orders of magnitude lower exchange current density in sharp contrast to acidic conditions [10–16]. This leads to performance losses in AMFCs with predicted overpotential penalties of 130–150 mV thereby requiring higher precious catalyst loadings [13,17]. In acid, HOR involves dissociative-adsorption of hydrogen (Tafel step: $\frac{1}{2}H_2 + M \rightarrow M\text{-}H_{ad}$) followed by direct oxidation to protons (Volmer step: $M\text{-}H_{ad} \rightarrow M + H^+ + e^-$) – leading to kinetics being primarily governed by M-H_{ad} surface energetics [11,18–20]. However, in alkaline media the adsorbed hydrogen intermediate (H_{ad}) subsequently reacts with hydroxide anions to form water (typically, Volmer step: $M\text{-}H_{ad} + OH^- \rightarrow M + H_2O + e^-$) [11]. Thus at high pH, HOR kinetics is dependent on the M-H_{ad} bond strength and/or the relevant processes furnishing reactive-hydroxide species [21–25]. While Volmer step is rate limiting in alkaline electrolyte, there is some controversy on whether the M-H_{ad} bond strength or the need for "reactive-OH_{ad}" species is the primary descriptor of the reaction. Correspondingly, there are two schools-of-thought to explain the slower alkaline HOR kinetics namely the i) hydrogen binding energy (HBE) theory [26–29], and ii) "reactive-OH_{ad}" species theory [22].

* Corresponding author.
E-mail address: s.mukerjee@northeastern.edu (S. Mukerjee).
[1] Present address: General Motors Corporation, Global Fuel Cell Activities, 895 Joslyn Avenue, Pontiac, MI 48340, USA.
[2] Present address: NanoTerra Inc., 737 Concord Avenue, Cambridge, MA 02138, USA.

http://dx.doi.org/10.1016/j.nanoen.2017.07.053
Received 20 May 2017; Received in revised form 29 July 2017; Accepted 30 July 2017
Available online 02 August 2017

Proponents of the former theory suggest that for any given catalyst surface, M-H_{ad} (M = Pt, Pd, Ir) bond strength is stronger in alkaline electrolyte than in acid which leads to HOR kinetics being slower at high pH conditions [26–31]. Further, alloying Pt with elements such as Ru is suggested to weaken the Pt-H_{ad} bond strength due to ligand-effect leading to higher alkaline HOR kinetics [28,32]. Proponents of the latter theory suggest that the non-availability of reactive-OH_{ad} species at the reaction interface is the major cause for slower alkaline HOR kinetics [22,23]. It was shown that alloying Pt with "oxophilic" alloying metals (e.g., Ru, Ni) increases HOR activity significantly due to the enhanced formation of (hydr)oxides on the alloying metal of the form Ru-OH_{ad} [22].

At the outset, we note that our experimental results clearly put us in favor of the reactive-OH_{ad} theory and not the HBE theory. Further, while there are certain merits to the reactive-OH_{ad} theory in its existing format the nature of the reactive OH_{ad} species is unlikely to be a simple specifically adsorbed Ru-OH_{ad} type moiety. Its conditions and source of formation requires detailed attention as this is a key intermediate causing high HOR overpotentials. In this article, we attempt to answer the following questions: i) Why is H_2-oxidation kinetics on Pt slower in alkaline electrolyte than in acid? ii) What is the nature of the reactive-OH_{ad} species responsible for HOR process at high pH? These learning are then applied towards the development and rational understanding of highly active bimetallic alloys. We accomplish this via a combination of electrochemical and spectroscopic measurements aided by a series of thought experiments to (i) understand the structural role of H_2O molecule in alkaline media, (ii) examine the plane of closest approach of OH^- anions, and (iii) scientifically interpret the commonality between H_{upd} stripping and alkaline HOR mechanisms.

2. Results and discussion

2.1. H_{UPD} deposition/stripping and HOR activity on Pt/C in alkaline electrolyte

We begin by comparing the electrochemical characteristics of Pt/C catalyst in dilute acid and alkaline electrolytes. Cyclic voltammetry (CV) of Pt/C in dilute acid and alkaline electrolytes (Fig. 1a) shows the expected features of polycrystalline Pt-surface with H_{upd} observed at potentials below 0.45 V followed by double-layer region (0.5–0.7 V) and then oxide formation above 0.7 V [13,33,34]. Upon closer examination, H_{upd} processes in alkaline electrolyte are observed to be shifted anodically compared to that in acid. For instance, the primary H_{upd} deposition/stripping peak (attributed to Pt(110) crystal planes [13,35,36]) observed at ~0.125 V in 0.1 M $HClO_4$ is shifted anodically to ~0.275 V in 0.1 M NaOH, representing a 150 mV overpotential (Fig. S1).

HOR polarization behavior of Pt/C (Fig. 1b) reflects a diffusion-controlled process in acid electrolyte even at very low potentials of ~0.05 V due to rapid kinetics [14]. Contrarily very high overpotential is observed in alkaline media [12,13]. At a 'kinetic current density (i_k)' of 1 A/mg_{Pt}, higher overpotential of ~170 mV is observed in 0.1 M NaOH compared to 0.1 M $HClO_4$ which clearly quantifies the sluggish HOR kinetics at high pH (Table S1). Further, HOR limiting current density is not achieved until ~0.4 V in alkaline media. There is a commonality observed between the high overpotentials required for both H_{upd} stripping and HOR on Pt in alkaline electrolyte compared to acid.

Recent studies have suggested that the anodic shift in H_{upd} stripping peak potential (E_{peak}) is an indication of a stronger Pt-H bond strength at high pH based on elementary H-binding energy (E_{M-H}) calculations using the equation $E_{M-H} = -E_{peak}F$ (F is the Faraday's constant) [26–29]. We note that the validity of such elementary calculations is questionable and overlooks some of the profound changes in the reaction mechanisms. Such a method would be valid only if the responsible reactions and the accompanying mechanisms in the Pt-H_{upd} process do not change as the pH traverses from acid to alkaline regime. This however, is not the case as explained in the next section [1]. Further, from basic principles of catalysis it is reasonable to understand that M-H_{ad} bond strength is different for various metal surfaces in any given electrolyte pH [19]. Nonetheless, it is intriguing and quite unproven to note that for any given metal surface, the M-H_{ad} bond strength of a neutral adsorbate (H_{ad}) becomes stronger with increasing pH. *Ab initio* theoretical studies used to calculate H-binding energies rarely account for the effect of changing pH [28]. Even those that did include the pH effect (via incorporation of the changing electron work function) did not take into consideration the effect of changing reaction mechanisms at high pH [37]. Further, we have calculated here the *d*-band vacancy parameter from X-ray absorption near edge spectra (XANES) of Pt L_3 and L_2 transitions which clearly shows only minor differences between acid and alkaline electrolytes at any given potential for Pt/C (Table S2 and Fig. S2). The *d*-orbital vacancy reflects the Pt electronic density of states near the Fermi level [38,39], and our experimental evidence suggests no major difference in the Pt-H_{upd} binding energies between acid and alkaline electrolytes for monometallic Pt/C catalyst.

2.2. Electrochemical double-layer model and quasi-specific adsorption of OH^- anions

We proceed by delving into the structural role of water and hydroxide anions in the alkaline electrochemical double-layer during H_{upd} deposition and stripping processes, respectively. In acid, Pt-H_{upd} formation simply involves the direct discharge of protons ($Pt + H^+ + e^- \rightarrow$ Pt-H_{upd}). In alkaline media H_{upd} formation occurs via $1e^-$ reduction of solvent water molecules ($Pt + H_2O + e^- \rightarrow$ Pt-$H_{upd} + OH^-$) which involves OH^- anions being produced as conjugate base in the compact part of double-layer [11]. *Classically*, this OH^- anion would be expected to diffuse away into bulk electrolyte. Given the complexity of electrochemical events in this process, we performed a series of thought experiments to sequentially visualize H_{upd} deposition/stripping mechanistic steps with detailed attention to double-layer structure. The *modern rendition* of the electrochemical double-layer structural evolution during H_{upd} deposition is shown in Fig. 1c (Stages 1 through 3 depicted with respect to the double-layer potential region, E_{dl}). In Stage 1 ($E < E_{dl}$), *prior to any electron transfer process* the adsorbed H_2O molecule could be imagined as orienting itself in the inner-Helmholtz Plane (IHP) with the hydrogen atoms facing the electrode due to the excess negative charge on the surface (flip-down state of water dipole [40]). After $1e^-$ transfer (Stage 2, $E < E_{dl}$), hydroxide species formed would not be completely cleaved from the water molecule but only be partially cleaved, and remain stabilized in the outer-Helmholtz plane (OHP) via a weak hydrogen-bond with the H_{upd} species. Such a structure is represented here as Pt-H_{upd}···$OH_{q\text{-}ad}$ cluster which encloses the hydroxide species in a *quasi-specifically adsorbed* state localized in the OHP. Only at further negative potentials (Stage 3, $E \ll E_{dl}$), OH^- anion could be considered to be completely cleaved followed by diffusion into the bulk. Hence, the overall H_{upd} deposition in dilute alkaline electrolytes is written as $Pt + H_2O + e^- \rightarrow$ Pt-H_{upd}···$OH_{q\text{-}ad} \rightarrow$ Pt-$H_{upd} + OH^-$. The reverse of this process (Fig. 1c, stages 3 through 1) occurs during anodic H_{upd} stripping – such that the approach of OH^- anion (Stage 3, $E \ll E_{dl}$) towards a negatively charged electrode surface would be limited to the OHP forming a hydrogen bond with H_{upd} in the fashion Pt-H_{upd}···$OH_{q\text{-}ad}$ (Stage 2, $E < E_{dl}$). This is followed by water molecule formation in Stage 1. *The crucial aspect of the modern rendition is that the H_{upd} deposition and stripping mechanisms in alkaline media progresses through a transition state structure composed of Pt-H_{upd}···$OH_{q\text{-}ad}$ involving both water molecule bond-breaking and bond-formation processes, respectively. These steps are simply not involved in acid electrolytes.*

H_{upd} stripping process explained above could essentially be extended to depict the HOR mechanism in alkaline media (Fig. 2) by simply replacing, for the sake of illustration, the H_{upd} species with the HOR intermediate (H_{ad}). Accordingly, Pt-H_{ad} intermediate (Stage 1,

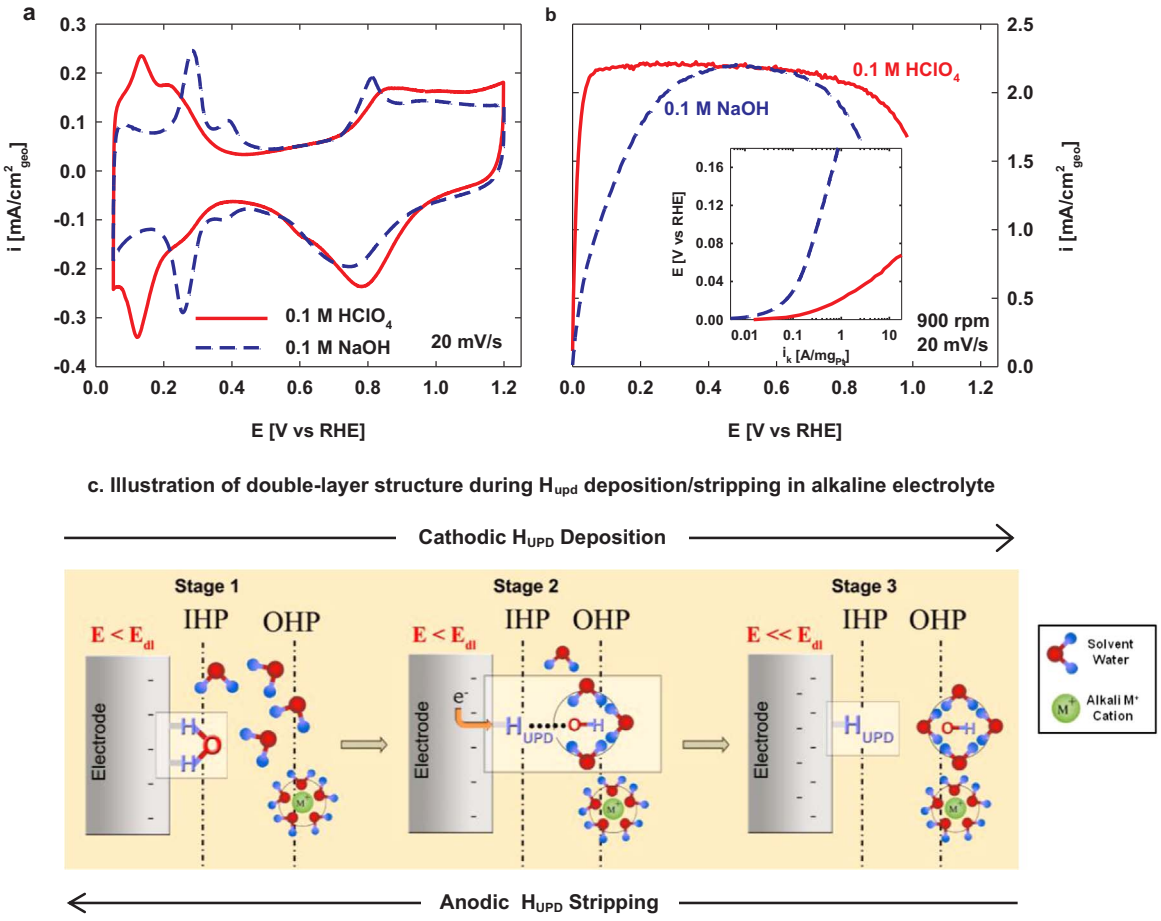

Fig. 1. HOR activity and H_{UPD} on Pt in Dilute Acid versus Alkaline Electrolytes. Comparison of electrochemical characteristics of TKK 46% Pt/C in 0.1 M $HClO_4$ and 0.1 M NaOH electrolytes at room temperature: (a) cyclic voltammetry in argon saturated electrolytes; (b) HOR polarization curve in H_2 saturated electrolytes; inset shows the mass-transport corrected HOR Tafel plots; (c) Schematic illustration of electrochemical double-layer structure during H_{UPD} deposition/stripping process in dilute alkaline electrolytes at various potentials with respect to the potential of double layer region (E_{dl}). All experiments carried out at room temperature.

E«E_{dl}) involves in a $1e^-$ oxidation process only at more anodic potentials (Stage 2–3, E < E_{dl}) to enable bond-formation in H_2O molecule via the transition state structure Pt-H_{ad}···$OH_{q\text{-}ad}$. As depicted in Stages 1 and 2, the negative charge on the electrode surface prevents the direct specific adsorption of OH^- anions but permits only quasi-specific interaction with H_{ad} from the OHP in the fashion Pt-H_{ad}···$OH_{q\text{-}ad}$. Recent studies suggest that specifically adsorbed Pt-OH_{ad} species are present on "Pt-defect sites" in the H_{upd} region on [22]. Pt L_3-edge XANES and delta-mu analysis discussed in Fig. S3, S4, and S5 show that in H_{upd} region, there is no formation of specifically adsorbed Pt-OH_{ad} which occurs only at potentials above ≥ 0.7 V.

In essence, the higher overpotential involved in the oxidation of Pt-H_{upd}/Pt-H_{ad} species to form water is inherent to the unique mechanistic steps in alkaline electrolyte. It is due to the higher activation energy required to draw negatively charged OH^- anions to the plane of closest approach (i.e. OHP) of a negatively charged electrode surface followed by the assemblage of an exclusive transition state structure of the form Pt-$H_{upd/ad}$···$OH_{q\text{-}ad}$ prior to enabling *bond-formation* in the product water molecule. On monometallic Pt surfaces, the "reactive-OH_{ad}" species is the quasi-specifically adsorbed ($OH_{q\text{-}ad}$) hydroxide moiety

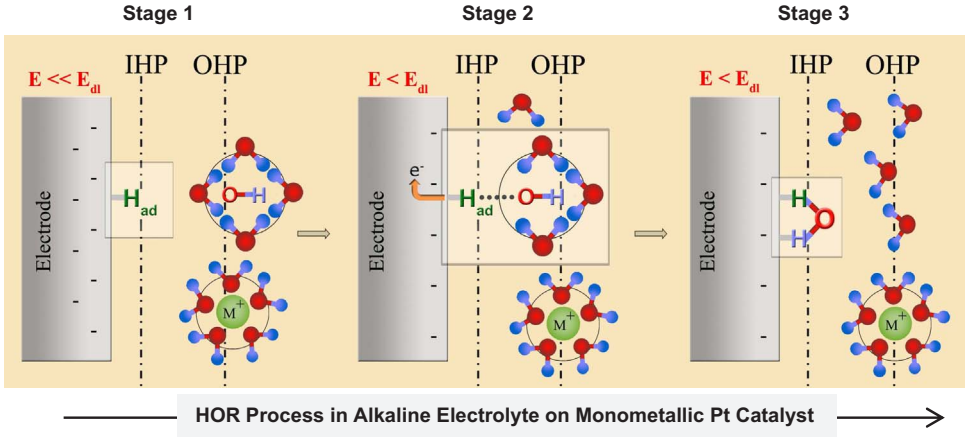

Fig. 2. Relationship between HOR electrocatalysis and the electrochemical double-layer structure in dilute alkaline electrolyte. Schematic illustration showing the potential dependent HOR reaction mechanism on monometallic Pt catalyst at various potentials.

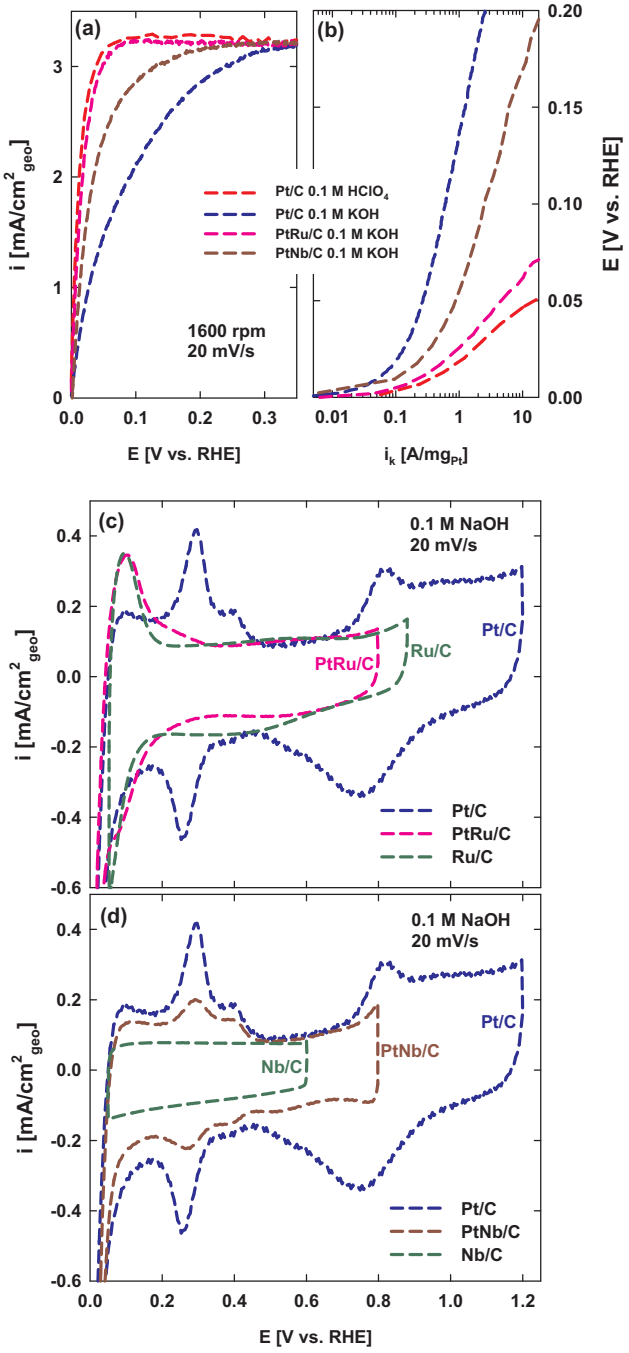

Fig. 3. HOR electrocatalysis on bimetallic catalysts in alkaline electrolyte. (a) HOR polarization curves, (b) Ohmic and mass transport corrected Tafel plots in H_2 saturated electrolytes and (c & d) cyclic voltammetry in argon saturated electrolyte. All measurements carried out at 40 °C.

localized in OHP. Interestingly, the above findings in alkaline HOR mechanism agrees with the recent development in alkaline H_2-evolution reaction (HER) mechanism where the *bond-breaking* of H_2O molecules was shown to be the major limitation for the sluggish HER kinetics on monometallic Pt surfaces [41].

2.3. HOR on bimetallic catalyst systems

Given the limitations of monometallic Pt catalyst being unable to furnish "reactive-OH_{ad}" species at a low enough potential, we proceed by developing bimetallic alloys for improved HOR activity and extending the double-layer structural model for better understanding of the reaction mechanisms [22,42]. Two alloying elements namely Ru and Nb were chosen such that Ru represents a metal surface capable of forming H_{upd} whereas Nb is a non-noble transition metal that is passivated with an oxide/hydroxide layer in aqueous electrochemical conditions. In both cases of bimetallic alloys (Fig. 3 and S6), a significant improvement in HOR activity is observed over that of Pt/C in alkaline pH. For instance, at $i_k = 1$ A/mg_{Pt} HOR overpotential on PtRu/C and PtNb/C is minimized by 110 mV and 80 mV respectively in comparison to Pt/C. HOR behavior of PtRu/C in alkaline electrolyte is similar to the diffusion controlled characteristics of Pt/C in acid. To rationalize the alkaline HOR mechanism of the bimetallic catalysts, we delve into the electrochemical and spectroscopic details of the reaction sequence.

CV of PtRu/C in 0.1 M NaOH (Fig. 3c) features a redox peak centered at ~0.1 V in the anodic scan followed by a tapering shoulder up to ~0.35 V. CV of Ru/C in 0.1 M NaOH (Fig. 3c) features a sharp redox peak in the potential region from 0.05 to 0.20 V followed by a slow rise in current-density above 0.20 V consistent with earlier observations on polycrystalline ruthenium [43–45]. A simple comparison of PtRu/C with Ru/C clearly shows that the peak at 0.1 V arises largely from the Ru component in the alloy. However, there is some controversy on the reactions responsible for this feature on PtRu, i.e., i) due to the high oxophilicity of Ru, some authors indicate the possibility of Ru-OH_{ad} below 0.2 V [43,44], and ii) due to a possible ligand effect of Ru on Pt some authors have suggested a "weakening of Pt-H_{upd}" by the Ru alloy which leads to a cathodic shift in the H_{upd} peaks in comparison to pure-Pt [28].

We clarify here that the reaction responsible for the anodic peak centered at 0.1 V on both PtRu/C and Ru/C arises due to Ru-H_{upd} formation. X-ray absorption near edge spectra (XANES) of Ru K-edge (Figs. S7 and S8) clearly shows that Ru nanoparticles are in a completely reduced state with no evidence of oxidation below 0.2 V; only above 0.20 V, the formation of specifically adsorbed Ru-OH_{ad} is evidenced on Ru surface. Significant improvement in HOR activity on PtRu/C catalyst is observed well below 0.2 V where no Ru-OH_{ad} formation is evidenced. Additionally, Delta-mu ($\Delta\mu$) technique, a surface sensitive spectral subtraction methodology in the XANES region [46,47] (see Supplementary Methods), is utilized here to identify the chemical nature of adsorbates on Ru at potentials relevant for HOR. The experimental $\Delta\mu$ ($\Delta\mu_e$) spectra of Ru (see Fig. 4a and S8) at 0.05 V and 0.2 V indicates a large positive feature from −40 to −20 eV followed by a negative dip at roughly −5 eV. As illustrated in Fig. 4a, the theoretical spectra ($\Delta\mu_t$) of a [Ru_6-H_{upd}] cluster used in the simulation clearly reflects the experimental spectroscopic signature obtained at 0.05 and 0.2 V (also see Figs. S6, S10). This yields unambiguous proof that the peak centered at 0.1 V on PtRu/C CV (Fig. 3c) can be ascribed to the Ru-H_{upd} process on PtRu/C catalyst.

Fig. 3d compares the CVs of PtNb/C and Nb/C. While Nb/C CV is essentially featureless, PtNb/C H_{upd} features are largely similar to Pt/C. A comparison of the H_{upd} feature of PtNb/C and Pt/C *in a single electrolyte* (i.e. 0.1 M NaOH) shows no shift in peak potentials. This is in good agreement with the *d-band* vacancy calculated from XANES spectra that show no major changes in the Pt electronic density of states at relevant potentials of 0.04 V due to Nb alloying indicating that the Nb does not affect the Pt-H binding energy (Table S2 and Fig. S11). While Nb K-edge XANES (Fig. 4b) edge position suggests an oxidation state of Nb^{2+}, a careful analysis of EXAFS also shows the presence of metallic Nb with a weak Nb-O(H) shoulder (Fig. S12). This indicates that Nb is present as a metallic Nb core with niobium oxyhydroxide surface ($Nb^{4+}O_x(OH_y)$) under in situ conditions giving an average oxidation state of Nb^{2+}. The above analysis suggests that the nature of the electrochemical processes on bimetallic PtRu/C and PtNb/C in alkaline media is complex and needs careful examination using multiple analytical techniques. While Ru exists in its metallic state enabling H_{upd} formation, the surface of Nb is largely covered with an oxyhydroxide layer - the implications of which for HOR are discussed in the next section.

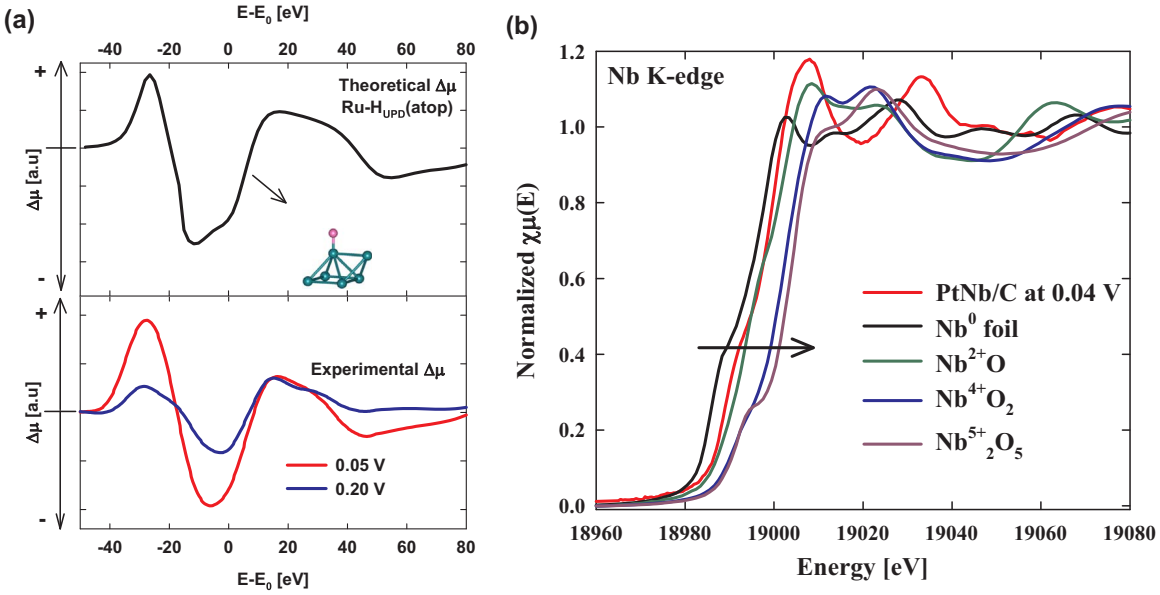

Fig. 4. Spectroscopic detection of adsorbate identity. (a) Theoretical Δμ ($\Delta\mu_t$) signature obtained by subtracting simulated XANES absorption probabilities of atop-H_{UPD} from atop-OH_{ad} on "Janin-type Ru_6 cluster". Experimental Δμ ($\Delta\mu_e$) signatures obtained by subtracting Ru K-edge XANES spectra at 0.05 V and 0.2 V from 0.3 V according to Δμ = μ(0.05 V or 0.20 V) - μ(0.30 V) in argon saturated 0.1 M NaOH electrolyte. Inset shows the structural models used in theoretical Δμ simulation. (b) Normalized XANES spectra of PtNb/C catalyst measured at Nb K-edge in argon saturated 0.1 M NaOH electrolyte.

2.4. Alkaline HOR mechanisms

This scenario brings us to some important conclusions on the HOR mechanisms in dilute alkaline electrolytes on mono- and bi-metallic catalysts. Briefly, on monometallic Pt/C (Fig. 5, Scheme 1) the higher HOR overpotential in alkaline media arises from the higher activation energy required to draw OH^- anion to the plane of closest approach (i.e. OHP) of a negatively charged electrode surface and subsequently form the transition state structure Pt-H_{ad}···$OH_{q\text{-}ad}$ leading to the bond formation of the final product water molecule. On monometallic Pt-surfaces, the nature of the reactive-OH_{ad} species is a complex quasi-adsorbed hydroxide moiety ($OH_{q\text{-}ad}$) involved in the formation of 'M-H_{upd}···$OH_{q\text{-}ad}$' cluster.

In the case of PtRu/C catalyst, we propose the following HOR mechanism based on the combination of surface sensitive spectroscopic studies (i.e., Δμ analysis) on Ru (which shows *no* evidence of specifically adsorbed Ru-OH_{ad} at potentials < 0.2 V relevant to HOR) and electrochemical double-layer structural model involving the formation of quasi-adsorbed hydroxide species. Ru enables the formation of quasi-specifically adsorbed reactive-hydroxide species of the form Ru-H_{upd}···$OH_{q\text{-}ad}$ via $1e^-$ reduction of water molecules at very low potentials relevant for HOR. The dissociatively adsorbed H_2 intermediate on Pt (Pt-H_{ad}) reacts with the quasi-specifically adsorbed reactive-hydroxide species (present in Ru-H_{upd}···$OH_{q\text{-}ad}$) to accelerate the *bond-formation* of product H_2O molecule at low potentials (Fig. 5, Scheme 2 – Bimetallic System I).

Finally, in cases of bimetallic systems where Pt is alloyed with transition metals such as niobium, gold [48], nickel [22] (Fig. S13), and copper [42] (Fig. S14) etc. *that do not form H_{upd} at high pH* but instead are passivated with a thin layer of oxide/hydroxide film, the promotion of HOR activity can be said to follow Scheme 3 (Fig. 5, Bimetallic System II). Only in such cases, electrocatalytic HOR involves a simpler bifunctional mechanism involving direct reaction between Pt-H_{ad} intermediate and OH_{ad} formed on an adjacent alloying element in the fashion $NbO_x(OH_y)$/Cu-OH_{ad}/Ni-OH_{ad}. To further buttress this argument on the effect of reactive-OH_{ad} on HOR, Fig. S15 shows the effect of acid cycling PtCo/C. With the loss of surface Co-O(H), a concomitant loss in HOR activity is also observed.

3. Conclusions

In summary, the rationale for high HOR overpotential lays in fundamental changes to the reaction mechanisms in alkaline electrolyte and not simply due to an increase in hydrogen-binding energy. HOR overpotential can be minimized by alloying a primary active site (such as Pt) capable of dissociatively adsorbing H_2 with either: i) a base

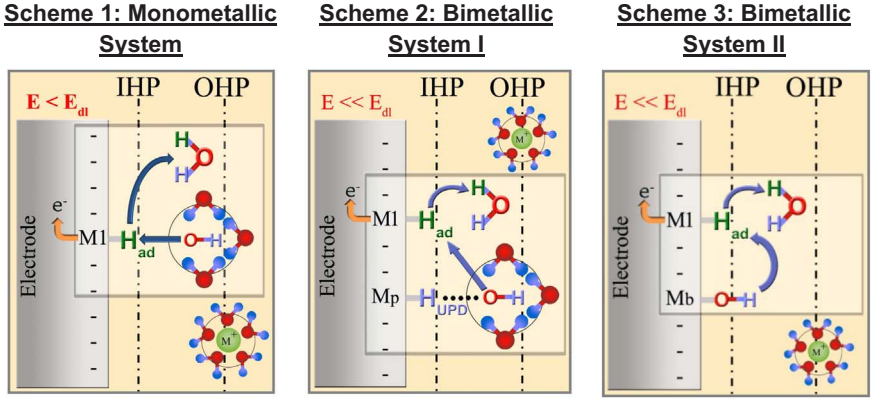

Fig. 5. Relationship between HOR electrocatalysis and electrochemical double-layer structure. Generic mechanistic reaction schemes for HOR in dilute alkaline electrolytes on mono- and bi-metallic catalyst systems. M1 represents a metal site capable of dissociatively adsorbing molecular hydrogen. In scheme 2, alloy element M_p represents a precious metal site capable of forming H_{upd} in alkaline electrolyte. In scheme 3, alloy element M_b represents a base-metal site passivated with adsorbed (hydr) oxide species in dilute alkaline electrolytes.

transition metal (M_b) that is passivated with a (hydr)oxide layer (M_b-OH_{ad}) at potentials low enough in the HOR region; [22,42] or ii) a metal, typically from precious metal-group (M_p) *capable of activating 1e⁻ reduction of water* to form M_p-H_{upd}···$OH_{q\text{-}ad}$ clusters. In such alloys, Pt-H_{ad} intermediate reacts either with OH_{ad} species formed on an adjacent base metal (M_b-OH_{ad}) as in the former case or in the latter case with $OH_{q\text{-}ad}$ species formed on the precious metal alloying element (M_p-H_{upd}···$OH_{q\text{-}ad}$) to enhance HOR kinetics.

4. Methods

4.1. Electrode preparations and electrochemical characterizations

Precious metal catalysts dispersed on high surface area carbon supports, namely TKK 46 wt% Pt/C and Johnson Matthey 20 wt% PtRu/C (bulk and surface Pt:Ru atomic ratio of 1:1) electrocatalysts were used as received. The metal contents and their atomic ratios of the as-received catalyst were verified using Energy Dispersive Analysis of X-rays. The average particle size of the Pt and PtRu catalysts were determined by both transmission electron microscopy and X-ray diffraction to be 2–3 nm and 4–5 nm, respectively. Ru/C with a nominal metal loading of 20% by weight and average XRD crystallite size of ~13 nm was synthesized in-house based on synthetic methodologies documented elsewhere [45]. PtNb/C catalyst was synthesized in-house using the procedure given in Supplementary Information. Fig. S16 shows the high resolution images and particle size distribution measurements of PtNb/C catalyst. Fig. S17 shows the X-ray diffraction patterns of the catalysts involved in this study. Electrochemical measurements were made using a rotating ring-disk electrode (RRDE) setup from Pine Instruments connected to an Autolab (Ecochemie Inc., model-PGSTAT 30) bi-potentiostat. Alkaline (0.1 M NaOH) and acidic (0.1 M $HClO_4$) electrolytes were prepared using sodium hydroxide pellets (semiconductor grade, 99.99%, Sigma-Aldrich) and double-distilled 70% perchloric acid (GFS Chemicals), respectively. Catalyst inks were prepared by ultrasonically dispersing the catalyst powder in a 1:1 (by volume) ratio of deionized water (Millipore, 18.2 MΩ cm) to isopropanol solution. Typical catalyst loadings employed were ~10 μg/cm ^{2} of the total precious metal content on 5 mm glassy carbon (GC) disk (Pine Instruments). GC disk was polished with 0.05 μm alumina (Buehler) followed by thorough rinsing with deionized water and dried at room temperature prior to use. Reversible Hydrogen Electrode (RHE) generated using the same electrolyte as the bulk was used as the reference electrode. All electrode potentials are addressed here with respect to the RHE scale in the electrolyte of interest, unless otherwise stated. All current values are normalized to the geometric area of the glassy carbon disk unless otherwise stated. (Details on the X-ray Absorption Spectroscopy experimental methods and Delta-Mu analytical methodology are presented in the Supplementary Information).

Acknowledgements

The authors deeply appreciate prior financial assistance from the Army Research Office under the Single Investigator grant for initiating this effort. Current financial support from ARPA-E (DE-AR0000688) lead by Pajarito Powders is deeply appreciated. Use of the synchrotron facilities at the National Synchrotron Light Source (NSLS), beamline X-11A at Brookhaven National Laboratory (BNL), Upton, NY and Stanford Synchrotron Radiation Light Source, (SSRL), beamline 2-2, National Accelerator Laboratory were both supported by the U.S. Department of Energy, Office of Science, Office of Basic Energy Sciences, former under Contract No. DE-SC0012704 and DE-AC02-76SF00515, respectively. Support from beamline personnel Drs. Syed Khalid, Nebojsa Marinkovic and Kaumudi Pandya at BNL is deeply appreciated and acknowledged.

Appendix A. Supporting information

Supplementary data associated with this article can be found in the online version at http://dx.doi.org/10.1016/j.nanoen.2017.07.053.

References

[1] S. Chu, A. Majumdar, Nature 488 (2012) 294.
[2] F.T. Wagner, B. Lakshmanan, M.F. Mathias, J. Phys. Chem. Lett. 1 (2010) 2204.
[3] J.S. Spendelow, D.C. Papageorgopoulos, Fuel Cells 11 (2011) 775.
[4] Fuel Cell Multi-Year Research, Development and Demonstration Plan. The US Department of Energy, Energy Efficiency and Renewable Energy. ⟨http://www.eere.energy.gov/hydrogenandfuelcells/mypp/pdfs/fuel_cells.pdf⟩.
[5] J.R. Varcoe, R.C.T. Slade, Fuel Cells 5 (2005) 187.
[6] G. Merle, M. Wessling, K. Nijmeijer, J. Membr. Sci. 377 (2011) 1.
[7] J.S. Spendelow, A. Wieckowski, Phys. Chem. Chem. Phys. 9 (2007) 2654.
[8] J. Suntivich, H.A. Gasteiger, N. Yabuuchi, H. Nakanishi, J.B. Goodenough, Y. Shao-Horn, Nat. Chem. 3 (2011) 546.
[9] N. Ramaswamy, U. Tylus, Q. Jia, S. Mukerjee, J. Am. Chem. Soc. 135 (2013) 15443.
[10] V.S. Bagotskii, N.V. Osetrova, J. Electroanal. Chem. Interfacial Electrochem. 43 (1973) 233.
[11] B.E. Conway, B.V. Tilak, Electrochim. Acta 47 (2002) 3571.
[12] T.J. Schmidt, P.N. Ross, N.M. Markovic, J. Electroanal. Chem. 524–525 (2002) 252.
[13] W. Sheng, H.A. Gasteiger, Y. Shao-Horn, J. Electrochem. Soc. 157 (2010) B1529.
[14] N.M. Markovic, B.N. Grgur, P.N. Ross, J. Phys. Chem. B 101 (1997) 5405.
[15] K.C. Neyerlin, W. Gu, J. Jorne, H.A. Gasteiger, J. Electrochem. Soc. 154 (2007) B631.
[16] J. Maruyama, M. Inaba, K. Katakura, Z. Ogumi, Z.-i. Takehara, J. Electroanal. Chem. 447 (1998) 201.
[17] P. Rheinländer, S. Henning, J. Herranz, H.A. Gasteiger, ECS Trans. 50 (2013) 2163.
[18] M.W. Breiter, Handbook of Fuel Cells, John Wiley & Sons, Ltd, 2010.
[19] K. Krischer, E.R. Savinova, 2nd edition, Handbook of Heterogeneous Catalysis 4 (2008), p. 1873.
[20] E. Skúlason, V. Tripkovic, M.E. Björketun, S. Gudmundsdóttir, G. Karlberg, J. Rossmeisl, T. Bligaard, H. Jónsson, J.K. Nørskov, J. Phys. Chem. C 114 (2010) 18182.
[21] T. Zhang, A.B. Anderson, J. Phys. Chem. C 111 (2007) 8644.
[22] D. Strmcnik, M. Uchimura, C. Wang, R. Subbaraman, N. Danilovic, V. van der, A.P. Paulikas, V.R. Stamenkovic, N.M. Markovic, Nat. Chem. 5 (2013) 300.
[23] M.T.M. Koper, Nat. Chem. 5 (2013) 255.
[24] S. St. John, R.W. Atkinson, K.A. Unocic, R.R. Unocic, T.A. Zawodzinski, A.B. Papandrew, ACS Catal. 5 (2015) 7015.
[25] S. St. John, R.W. Atkinson, R.R. Unocic, T.A. Zawodzinski, A.B. Papandrew, J. Phys. Chem. C 119 (2015) 13481.
[26] J. Durst, A. Siebel, C. Simon, F. Hasche, J. Herranz, H.A. Gasteiger, Energy Environ. Sci. 7 (2014) 2255.
[27] W. Sheng, Z. Zhuang, M. Gao, J. Zheng, J.G. Chen, Y. Yan, Nat. Commun. (2015) 6.
[28] Y. Wang, G. Wang, G. Li, B. Huang, J. Pan, Q. Liu, J. Han, L. Xiao, J. Lu, L. Zhuang, Energy Environ. Sci. 8 (2015) 177.
[29] J. Zheng, Z. Zhuang, B. Xu, Y. Yan, ACS Catal. 5 (2015) 4449.
[30] J. Zheng, W. Sheng, Z. Zhuang, B. Xu, Y. Yan, Sci. Adv. (2016) 2.
[31] J.N. Schwämmlein, H.A. El-Sayed, B.M. Stühmeier, K.F. Wagenbauer, H. Dietz, H.A. Gasteiger, ECS Trans. 75 (2016) 971.
[32] K. Elbert, J. Hu, Z. Ma, Y. Zhang, G. Chen, W. An, P. Liu, H.S. Isaacs, R.R. Adzic, J.X. Wang, ACS Catal. 5 (2015) 6764.
[33] U.A. Paulus, A. Wokaun, G.G. Scherer, T.J. Schmidt, V. Stamenkovic, N.M. Markovic, P.N. Ross, Electrochim. Acta 47 (2002) 3787.
[34] N. Ramaswamy, S. Mukerjee, J. Phys. Chem. C 115 (2011) 18015.
[35] N.M. Markovic, H.A. Gasteiger, P.N., Jr Ross, J. Phys. Chem. 100 (1996) 6715.
[36] R. Subbaraman, D. Strmcnik, V. Stamenkovic, N.M. Markovic, J. Phys. Chem. C 114 (2010) 8414.
[37] J. Rossmeisl, K. Chan, R. Ahmed, V. Tripkovic, M.E. Bjorketun, Phys. Chem. Chem. Phys. 15 (2013) 10321.
[38] S. Mukerjee, S. Srinivasan, M.P. Soriaga, J. Electrochem. Soc. 142 (1995) 1409.
[39] S. Mukerjee, J. McBreen, J. Electrochem. Soc. 143 (1996) 2285.
[40] J.O.M. Bockris, M.A. Habib, Electrochim. Acta 22 (1977) 41.
[41] R. Subbaraman, D. Tripkovic, D. Strmcnik, K.-C. Chang, M. Uchimura, A.P. Paulikas, V. Stamenkovic, N.M. Markovic, Science 334 (2011) 1256.
[42] S.M. Alia, B.S. Pivovar, Y. Yan, J. Am. Chem. Soc. 135 (2013) 13473.
[43] J. Ohyama, T. Sato, Y. Yamamoto, S. Arai, A. Satsuma, J. Am. Chem. Soc. 135 (2013) 8016.
[44] N.A. Anastasijevic, Z.M. Dimitrijevic, R.R. Adzic, J. Electroanal. Chem. Interfacial Electrochem. 199 (1986) 351.
[45] N. Ramaswamy, R.J. Allen, S. Mukerjee, J. Phys. Chem. C 115 (2011) 12650.
[46] M. Teliska, W.E. O'Grady, D.E. Ramaker, J. Phys. Chem. B 109 (2005) 8076.
[47] S. Mukerjee, T. Arruda, Mod. Asp. Electrochem. 50 (2010) 503.
[48] D. Strmcnik, K. Kodama, D. van der Vliet, J. Greeley, V.R. Stamenkovic, N.M. Markovic, Nat. Chem. 1 (2009) 466.

Dr. Nagappan Ramaswamy is currently a Research Engineer at the Global Fuel Cell Activities Division, General Motors Corporation located at Pontiac, Michigan USA. Dr. Ramaswamy received a Bachelor of Chemical & Electrochemical Engineering degree from Central Electrochemical Research Institute, India in 2005 and a Ph.D. degree in Physical Chemistry from Northeastern University, USA in 2011. His doctoral thesis involved the investigation of precious and non-precious electrocatalyst materials in acid and alkaline electrolytes with a particular emphasis on unravelling the fundamental relationships between electrochemical double layer structure and catalytic mechanisms.

Ms. Shraboni Ghoshal received her Bachelor degree in Chemistry from University of Calcutta, and Master degree in Chemistry from Indian Institute of Technology, Kanpur. She earned a Master degree in Chemistry and Chemical Biology from Rutgers, the State University of New Jersey. She is currently pursuing her Ph.D. degree in Prof. Sanjeev Mukerjee at Northeastern University. Her research work involves catalyst designing for oxygen reduction reaction and hydrogen oxidation reaction.

Dr. Michael Bates obtained his Ph.D. in Physical Chemistry from Northeastern University in 2015. His research involved development of transition metal alloy and oxide nanoparticles for reversible hydrogen and oxygen electrodes, primarily for alkaline water electrolysis. He is currently a senior scientist at Nano Terra, a materials science R & D firm developed from Dr. George Whitesides' lab at Harvard, where he works on a diverse range of projects including: piezo-electric transducers, hydrogels for aerosol drug delivery, optically reflective magnetic coatings and electrochemical biosensors for patient diagnostics and human performance monitoring.

Dr. Qingying Jia (MS and BS in Physics from Beijing University) is currently a Research Assistant Professor at Northeastern University. Dr. Jia obtained his Ph.D. in Material Sciences at Illinois Institute of Technology, USA in 2010. Dr. Jia's research centers on synchrotron-based in situ X-ray absorption spectroscopy (XAS) characterization of (electro)catalysts with applications to fuel cells and batteries.

Miss Jingkun Li received her Bachelor degree in Applied Chemistry from Hefei University of Technology in 2009 and Master degree in Chemical Engineering from Shanghai Jiao Tong University in 2012 under the advisory of Prof. Zifeng Ma. She is currently pursuing her Ph.D. degree under the supervision of Prof. Sanjeev Mukerjee at Northeastern University focusing on oxygen reduction reaction.

Dr. Sanjeev Mukerjee is a Professor in the Department of Chemistry and Chemical Biology (Northeastern University); where he has been since September of 1998. He also heads the newly created center for Renewable Energy Technology and its subset the Laboratory for Electrochemical Advanced Power (LEAP). He is the author of 130 peer-reviewed publications with a current H-index of 53 and is a fellow of the Electrochemical Society. He has given numerous invited and keynote presentations in various national and international meetings and holds five US and international patents. He also serves on the scientific advisory boards of three companies.